Available online at www.sciencedirect.com
ScienceDirect
Applied Catalysis A: General 337 (2008) 138–147
APPLIED CATALYSIS A: GENERAL
www.elsevier.com/locate/apcata

Preparation, characterization and activities of the nano-sized Ni/SBA-15 catalyst for producing CO_x-free hydrogen from ammonia

Hongchao Liu [a,b], Hua Wang [a], Jianghan Shen [a,b], Ying Sun [a,b], Zhongmin Liu [a,*]

[a] *Laboratory of Applied Catalysis, Dalian Institute of Chemical Physics, Chinese Academy of Sciences, 457 Zhongshan Road, Dalian 116023, Liaoning, PR China*

[b] *Graduate School of the Chinese Academy of Sciences, Beijing 100049, PR China*

Received 19 May 2007; received in revised form 5 December 2007; accepted 5 December 2007
Available online 15 December 2007

Abstract

Ni/SBA-15 catalysts that are used in ammonia decomposition to produce CO_x-free hydrogen were prepared by a deposition–precipitation (DP) method and investigated by N_2 adsorption/desorption, XRD, TEM and H_2-TPR techniques. The results show that not only the nano-sized nickel particles with narrow distribution could be obtained, but also the ordered mesostructures of the Ni/SBA-15 catalysts could be achieved during the preparation process. The amount of formed nickel phyllosilicate increases with prolonging the DP time, while surface areas and pore sizes of samples decrease relatively. These Ni/SBA-15 catalysts exhibit higher performance than other Ni-based catalysts and even some supported Ru catalysts. Ammonia conversion is more than 96% at 873 K with $GHSV_{NH_3}$ of 46,000 ml/h g-cat. Additionally, the Ni/SBA-15 catalyst is very stable during catalytic evaluation operation due to the strong interactions between nickel grains and SBA-15 support.

Keywords: Deposition–precipitation method; Ni/SBA-15; CO_x-free hydrogen; Ammonia decomposition

1. Introduction

The on-site hydrogen production for proton exchange membrane fuel cells (PEMFC) has attracted much attention based on the need for environmental protection [1]. The hydrogen produced from carbonaceous substances (e.g. methanol, methane) is inevitably accompanied by CO_x ($x = 1, 2$) as a byproduct that degrades the lifetime of PEMFC even at extremely low concentrations [1,2]. As an alternative method, photoelectrolysis and photocatalysis of water utilizing renewable sources (e.g. solar energy) seem to be attractive for CO_x-free hydrogen generation, but some major breakthroughs (e.g. hydrogen production rates, stability of catalysts) are needed currently [3]. Therefore, the CO_x-free hydrogen production from ammonia decomposition is preferable because there is no generation of CO_x, and trace unconverted ammonia could be reduced to ppb levels by using specific adsorbents [1]. Moreover, ammonia storage and delivery can be more readily handled [4,5]. Therefore, many investigators have focused on supported group VIII metals (Ru, Pd, Ir, Pt, Rh Ni, Fe, etc.) catalysts for ammonia decomposition [1,2,6–12]. Recently, a high-throughput screening technique has been used in our laboratory to test catalytic samples for this reaction [13,14]. Among these investigations, supported Ru catalysts [2,6–9] are the most active, although the cost is still a major drawback. The low cost and long-proven performance of supported Ni catalysts, therefore, warrant efforts to optimize these catalysts as alternatives of Ru-based catalysts in ammonia decomposition for generation of CO_x-free hydrogen [9–15]. Conventional coprecipitation methods or impregnation techniques were usually applied to prepare supported Ni catalysts for ammonia decomposition [1,2,9–15]. Coprecipitation yields catalysts with narrow size distribution, but is not easy to control and reproduce. The impregnation method can prepare catalysts with high metallic loading whereas it cannot always provide the desired active-phase distribution, loading and/or dispersion [16].

Recently, a deposition–precipitation (DP) method, developed by Gues and van Veen [16] and extensively investigated by Che and co-workers [17–20], has been introduced to prepare Ni/SiO_2 catalysts. This method is based on the precipitation of a Ni(II)

* Corresponding author. Tel.: +86 411 84685510; fax: +86 411 84685510.
E-mail address: liuzm@dicp.ac.cn (Z. Liu).

0926-860X/$ – see front matter © 2007 Elsevier B.V. All rights reserved.
doi:10.1016/j.apcata.2007.12.006

phase onto silica with a slow, homogeneous basification process of the solution containing the metal precursor and the support by urea hydrolysis at 363 K. The nature of the Ni(II) phase deposited on the surface of the support depends on DP time and on silica surface area, and 1:1 nickel phyllosilicate and nickel hydroxide will be produced during the DP procedure [18]. After reduction in hydrogen, the Ni(II) phase deposited on the surface of the support leads to highly dispersed Ni particles with a narrow size distribution and a high degree of thermal stability [19,20].

SBA-15, discovered as an ordered mesoporous silica a few years ago, presents some advantages as a catalyst support, such as high surface area (600–1000 m^2/g) and a hexagonal structure of mesopores with size 4.6–30 nm and thicker walls (3.1–6.4 nm) [21]. Unfortunately, few investigations of Ni/SBA-15 catalysts prepared with the DP method were reported [22]. Therefore, it is interesting to employ SBA-15 as a support in combination with advantages of DP method for preparing highly active ammonia decomposition catalysts with high dispersion, narrow particle distribution and high thermal stability. A series of Ni/SBA-15 catalysts have been prepared by the DP method and used to produce CO_x-free hydrogen from ammonia decomposition in the present work.

2. Experimental

2.1. Catalyst preparation

The Ni/SBA-15 catalysts were prepared by the DP method developed and described by Burattin [17–20]. First, 300 ml of an aqueous solution of nickel nitrate ($Ni(NO_3)_2{\cdot}6H_2O$, 0.14 mol) and nitric acid (0.02 mol) was prepared. Then 250 ml of this solution was used to make a suspension with freshly calcinated SBA-15 (1.95 g supplied by Jilin University) that was subsequently heated to 328 K in a thermostat vessel. The other 50 ml of solution was employed to dissolve the chosen amount of urea and this combination was mixed with the suspension. Subsequently, the mixture was heated to 363 K, where the OH^{-1} group could be provided to initiate the deposition–precipitation of nickel onto SBA-15 due to the hydrolysis of urea. After a chosen DP time, the suspension was stirred at 328 K for 10 min and then cooled to 298 K. After filtration, the solid was washed with deionized water three times. Finally, the sample was dried at 383 K for 24 h, and then calcinated from ambient to 823 K (heating rate: 1 K/min, 3 h at the final temperature) in air.

In the present study, the catalysts were identified as ''Ni/SBA-15(x)'', in which the symbol x represents the DP time (h). Moreover, a Ni/SBA-15 sample with 10% Ni loading was prepared by the traditional wet impregnation method, and named as 10% Ni/SBA-15(r). This sample has been regarded as the reference catalyst to study the effects of various catalyst preparation methods.

2.2. Catalyst characterization

The chemical compositions were determined with a Philips Magix X spectrometer. The powder XRD patterns were recorded with a D/max-rb-type X-ray diffractometer using monochromatic Cu Kα radiation (λ = 1.5418). The texture properties of support and catalysts were measured on a NOVA-4000 physical adsorption instrument using liquid nitrogen as adsorbate at 77 K. Prior to measurements, these samples were degassed in vacuum at 573 K for 4 h to remove physically adsorbed components. Transmission electron microscopy (TEM) images were obtained using a JEOL JEM2000EX electron microscope with an accelerating voltage of 120 kV. Prior to TEM measurements, the samples were ultrasonically dispersed into anhydrous ethanol for 5 min.

H_2-TPR experiments were conducted with an AutoChem 2910 chemisorption analyzer (Micromeritics). For the H_2-TPR experiments, each sample (30 mg) was calcinated at 773 K for 30 min to eliminate any impurities (e.g. H_2O) and then cooled to ambient temperature. TPR profiles were obtained under a flow of 10% H_2/Ar (40 ml/min) from 313 to 1073 K at a heating rate of 10 K/min. The consumption of hydrogen was monitored with a thermal conductivity detector (TCD).

2.3. Catalyst evaluation

Each catalytic test was carried out in a fixed-bed continuous flow quartz reactor (6 mm internal diameter) at atmospheric pressure. The reaction temperature was controlled by a programmable temperature controller and measured with a moveable K type thermocouple in the catalyst bed. The rate of the reaction was found to be the same for constant gas-hourly space velocity ($GHSV_{NH_3}$) when the mass of catalyst (40–60 mesh) and the flow rate were changed, indicating the absence of any mass transfer (mainly pore diffusion) effect. For complete reduction at relatively slow rates, the catalyst (0.1 g) was reduced in situ with 25% H_2/He flow at a defined temperature for 5 h prior to the reaction, and then purged with He for 30 min. The reaction temperature was in the range from 723 to 923 K, and the flow rate of ammonia was 50 ml/min ($GHSV_{NH_3}$ = 30,000 ml/g-cat h). Analysis of the effluent was performed with an on-line Varian CP-3800 gas chromatograph equipped with a Poropak-N column and a thermal conductivity detector.

3. Results and discussion

3.1. Physicochemical characterization

3.1.1. BET surface area and pore structure

Table 1 shows the physical properties of support and Ni/SBA-15 catalysts prepared by DP method. It is apparent that the nickel deposition has a notable impact on the catalyst properties. Compared to SBA-15, the surface area, pore volume and diameter of catalysts prepared with DP method decrease obviously. With increasing DP time, the nickel loading increases, and consequently the surface area and pore volume of samples both decrease relatively, while on the contrary the wall thickness increases. This result indicates that most loaded species had entered into the pore system and that the DP time has a considerable effect on the physical properties

Table 1
Physical properties of support and Ni/SBA-15 catalysts prepared by deposition–precipitation method

Catalyst	DP time (h)	Ni (wt.%)	S_{BET} (m^2/g)	V_P (cm^3/g)[a]	D_P (nm)[b]	E (nm)[c]
SBA-15	–	–	838.5	1.26	6.59	4.45
Ni/SBA-15(2)	2	18.0	527.1	0.82	4.90	6.51
Ni/SBA-15(3)	3	23.4	365.0	0.54	4.31	6.74
Ni/SBA-15(4)	4	26.2	287.7	0.36	3.84	7.18

[a] Pore volume calculated from the desorption branch of N_2 physisorption isotherm.
[b] BJH desorption average pore diameter.
[c] Wall thickness of samples estimated according to the expression: $E = \frac{2d_{(100)}}{\sqrt{3}} - d_{pore}$.

of samples. Fig. 1 shows the N_2 adsorption–desorption isotherms of all samples. The adsorbed volume and pore diameter decrease with the increasing loading, in agreement with that shown in Table 1. Moreover, all the samples show a typically reversible-type IV isotherm, indicating that the mesoporous structures of the samples were maintained.

3.1.2. X-ray diffraction (XRD)

Fig. 2 shows the XRD patterns of the dried samples. The intense main diffraction peak and two weak peaks in Fig. 2(A), which are assigned to {1 0 0}, {1 1 0} and {2 0 0} reflection, respectively, imply that dried samples have retained ordered hexagonal mesostructures. However, a shift of these diffraction peaks to higher 2θ values is identified for dried samples, possibly due to the contraction of support framework with increasing DP time in the DP process [23]. Moreover, the intensities of the reflection peaks such as d(1 0 0), d(1 1 0) and d(2 0 0) are gradually attenuated (Fig. 2(A)) with increasing DP time. The reduction of reflections may be caused by a degradation of the hexagonal arrangement of SBA-15 pores [24] or by a dilution of silica with continuous incorporation of nickel as a consequence of higher absorption factor for X-rays than silicon [25]. Fig. 2(B) shows the high angle XRD patterns of the dried samples. A broad diffraction peaks at 2θ between 20° and 30° are attributed to the peak of siliceous material. In addition, two new asymmetric diffraction peaks appeared at $2\theta = 33.9°$ and 60°, which can be assigned either to 10 and 11 reflections of turbostratic nickel hydroxide or to 13–20 and 06–33 reflections of ill-crystallized 1:1 nickel phyllosilicate [17,26]. The intensity of these reflections increase with the DP time, which is consistent with the increasing amount of nickel deposited.

Fig. 3 shows the XRD patterns of the samples calcinated in air at 823 K for 3 h. The variation of low angle XRD with DP time is in accordance with the results of dried samples. With

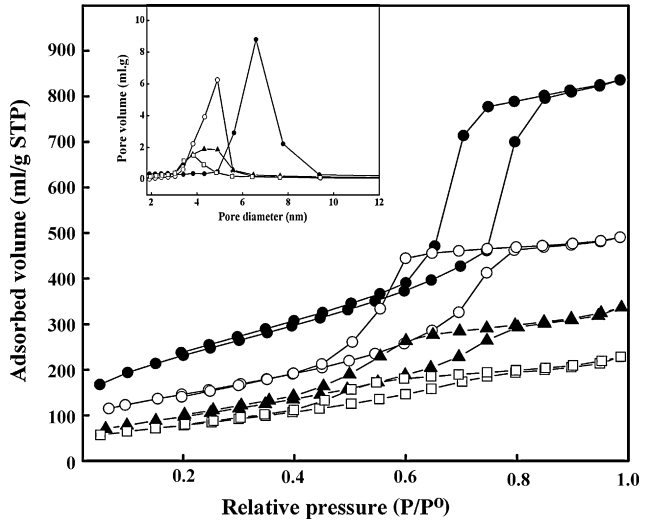

Fig. 1. N_2 adsorption–desorption isotherms of (●) SBA-15, (○) Ni/SBA-15(2), (▲) Ni/SBA-15(3) and (□) Ni/SBA-15(4).

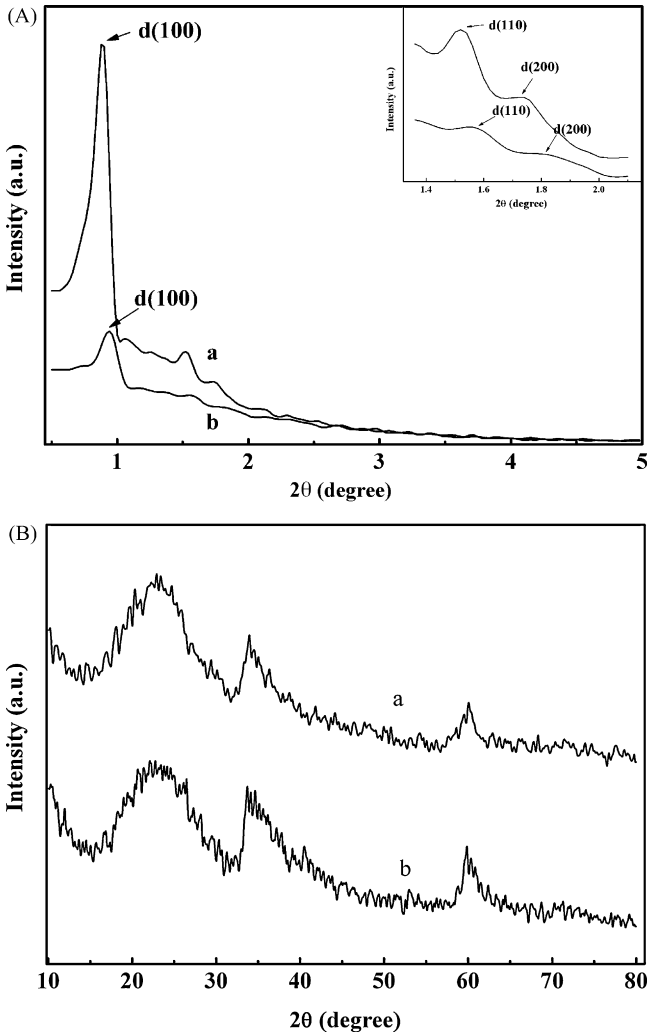

Fig. 2. XRD patterns of dried samples. (a) Ni/SBA-15(2) and (b) Ni/SBA-15(3).

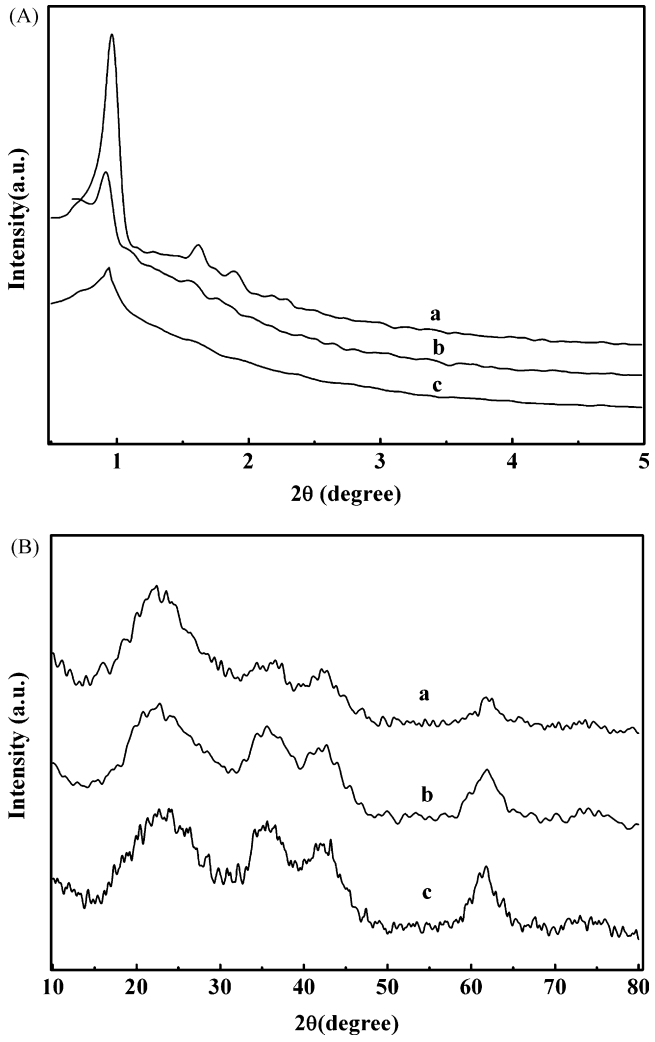

Fig. 3. XRD patterns of calcinated samples. (a) Ni/SBA-15(2), (b) Ni/SBA-15(3) and (c) Ni/SBA-15(4).

silica support, XRD patterns (Fig. 3(B)) show three new broad peaks at $2\theta = 37^\circ$, 43° and 62° which are characteristic peaks of NiO. Additionally, the peaks of NiO gradually increase with the DP time, which indicates that the amount of detectable crystalline NiO is enhanced. This is in line with XRF result in Table 1. The 10% Ni/SBA-15(r) sample was also characterized by XRD techniques: the NiO particle size of the reference sample is much larger than that of the samples prepared with DP method according to the line broadening of the main X-ray diffraction peak of NiO.

Fig. 4 shows the XRD patterns of Ni/SBA-15 catalysts reduced under different temperatures. The peaks at $2\theta = 44^\circ$, which can be assigned as the characteristic peaks of Ni^0, can be observed obviously, and their peak width at half height lessen with increasing of reduction temperature. The result suggests that the morphology of nickel particle changes with reduction temperatures when the catalysts were reduced at higher temperatures for a long time. In addition, one broad peak originating from NiO could be observed when the reduction temperature is 773 K, indicating that the reduction is incomplete at the lower temperature.

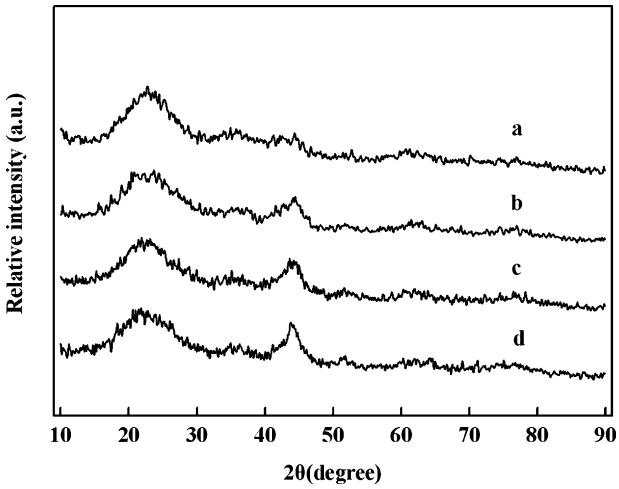

Fig. 4. XRD patterns of Ni/SBA-15 catalysts reduced at different temperatures. (a) 773 K, (b) 873 K, (c) 923 K and (d) 973 K.

3.1.3. Transmission electron microscopy (TEM)

Fig. 5 displays one representative TEM image of the dried sample. One can see that lamellar fibrous phases are dispersed on the silica surface with random orientations. The lamellar phases might be nickel phyllosilicate or nickel hydroxide or the mixtures of them because they are both lamellar compounds as we can see from the results of XRD patterns (Fig. 2B).

Figs. 6 and 7 exhibit the micrographs of fresh catalysts and used catalysts, respectively. It is obvious that the mesoporous structure of SBA-15 has been preserved for both fresh catalysts and used catalysts. Nano-size nickel metal particles with 4–7 nm diameter and narrow nickel particle distributions could be observed in Figs. 6 and 7. We can detect few clear changes of pore structure of catalysts and size/distribution of nickel particles from fresh catalysts to used catalysts via the comparison of TEM images between fresh catalysts and relevant used ones. Furthermore, we can conclude that the transformation of nickel phyllosilicate or nickel hydroxide or the mixtures of them to metallic oxides and metallic nickel atom arose due to the calcination and consequently the reduction processes, according

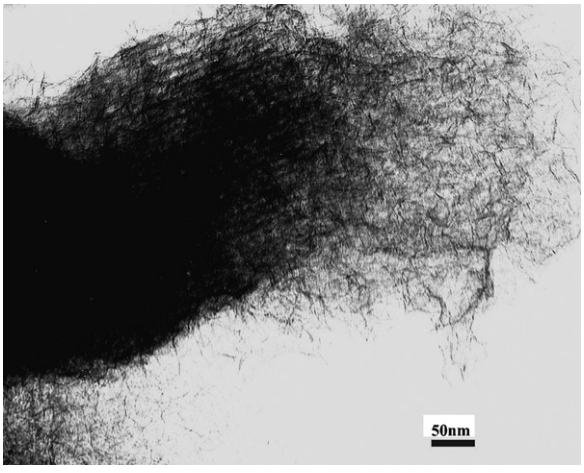

Fig. 5. TEM images of dried samples.

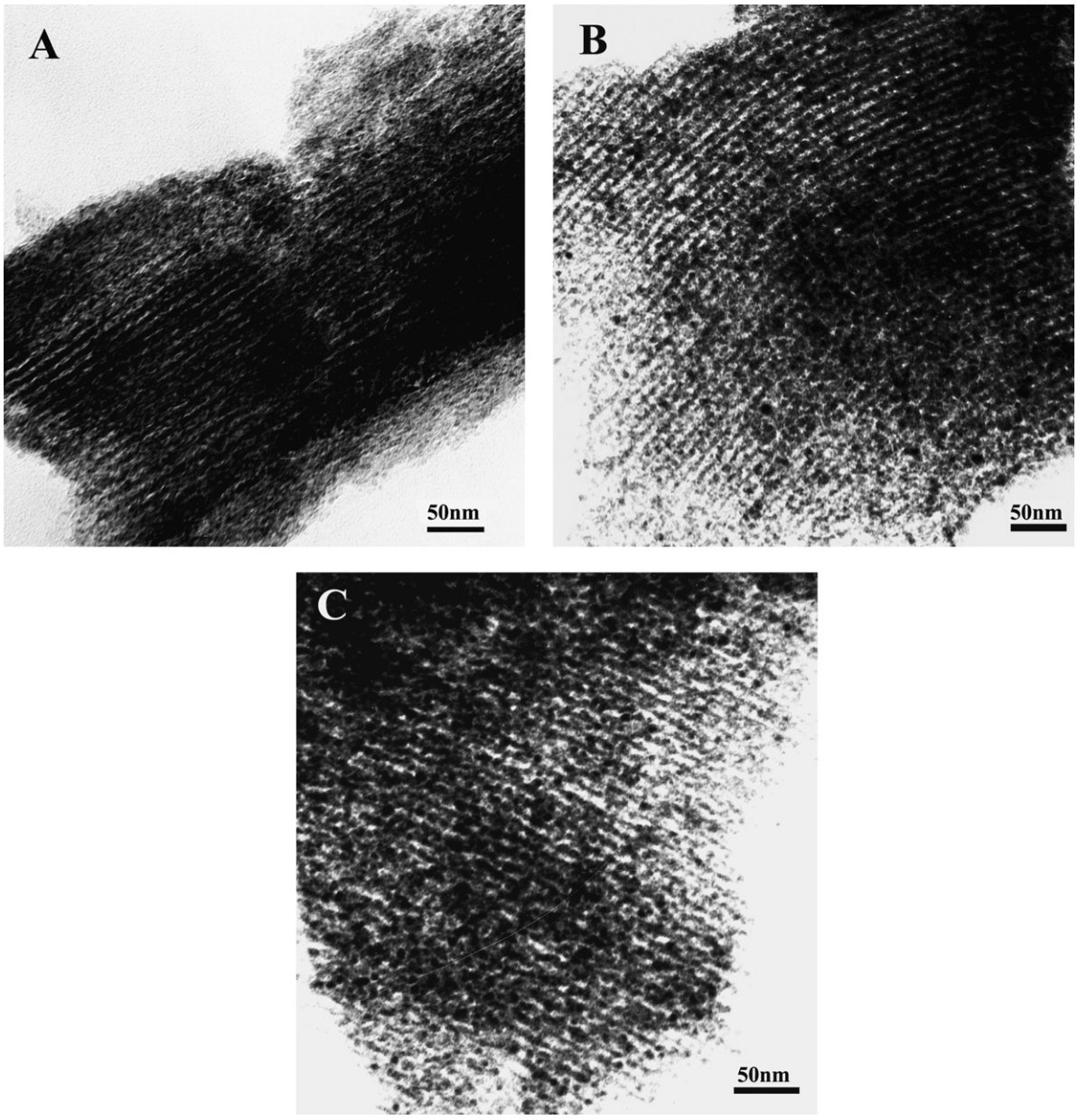

Fig. 6. TEM images of fresh catalysts reduced in 25% H_2/He at 773 K for 5 h. (A) Ni/SBA-15(2), (B) Ni/SBA-15(3) and (C) Ni/SBA-15(4).

to the results of XRD patterns (Figs. 2B and 3B) and TEM images (Figs. 5 and 6).

The results of N_2 adsorption–desorption isotherm and TEM (Fig. 5) indicate that the hexagonal arrangement of SBA-15 frameworks was retained for both dried samples and reduced samples. Therefore, we could conclude that the reduction of relative peaks (Figs. 2 and 3) was mainly caused by the effect of dilution with continuous incorporation of nickel as a consequence of having a higher absorption factor for X-rays than silicon has.

Fig. 8 gives the TEM images of the Ni/SBA-15 catalysts reduced under different temperatures. Larger nickel particles appear with raising the reduction temperatures whereas the ordered mesostructure of catalysts is largely retained. The results indicate that the morphology of nickel particles changes even when the texture of the catalysts is not much changed.

3.1.4. H_2 temperature programmed reduction (H_2-TPR)

Fig. 9 shows the H_2-TPR curves of Ni-based samples calcinated at 873 K for 3 h. For the 10% Ni/SBA-15(r) sample, three peaks were observed: small shoulder peaks at about 570 K and two major peaks at around 650 K and 850 K, respectively. Considering the evidence presented in previous investigations [27–29], these two peaks at 570 K and 650 K could be assigned, respectively to large particles and small particles of NiO which, although dispersed by the support, do not form significant chemical oxides with the underlying support surface. That is, most of the nickel oxide is deposited on the surface of silica in 10% Ni/SBA-15(r) sample. Moreover, the peak at around 850 K could be attributed to a strong interaction between Ni^{2+} and support to form a few surface layers of silicate-type compounds [30].

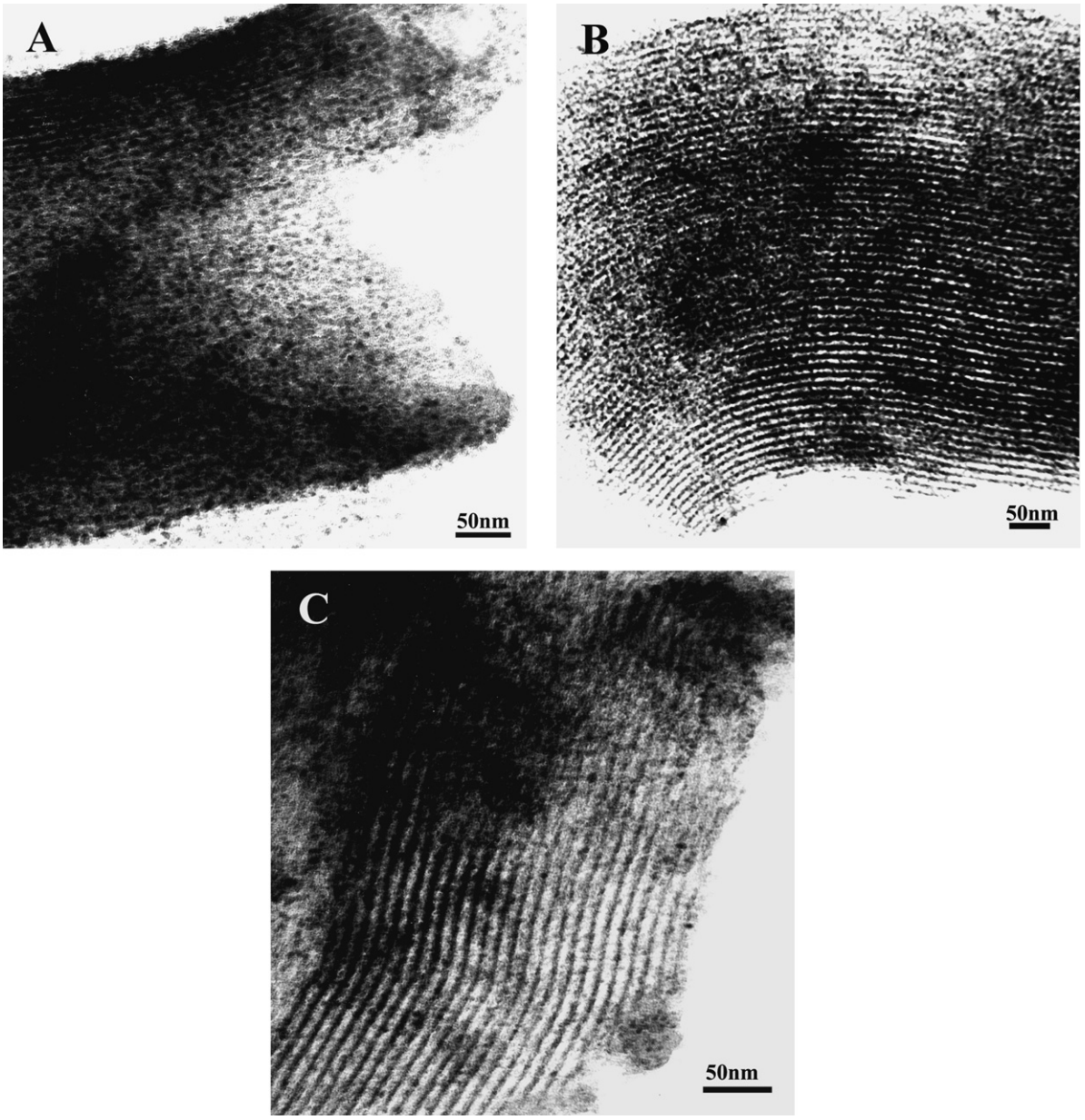

Fig. 7. TEM images of used catalysts. (A) Ni/SBA-15(2), (B) Ni/SBA-15(3) and (C) Ni/SBA-15(4).

It is obvious that the H_2-TPR curves of the samples prepared with DP method are different from that of the 10% Ni/SBA-15(r). Only two peaks appeared: one broad peak at high temperature and a shoulder peak at low temperature, and the small shoulder peak around 570 K that appears in the reference 10% Ni/SBA-15(r) catalyst disappeared in all the DP method prepared samples, which means that large particles of Ni species were restricted and that the active compounds were highly dispersed on the supports. For the Ni/SBA-15(2) sample, one shoulder peak around 670 K and one broad peak around 817 K are observed. XRD patterns (Fig. 2B) and TEM image (Fig. 5) show the formation of nickel phyllosilicate or nickel hydroxide for the dried sample, and crystalline NiO phases were presented when the dried samples were calcinated at 823 K for 3 h (Fig. 3B). Therefore, different peaks could be assigned to different interactions between the NiO and Si ions: the broad peak should be considered to be associated with the nickel phyosilicate, while the shoulder peak is correlative to the nickel hydroxide. We can claim this by combining these results with those obtained previously from SiO_2 supported nickel hydroxide and nickel phyllosilicate [17–20].

3.2. Catalytic activity

3.2.1. Effect of the DP time on catalytic performance

The effect of the DP time on reaction activity of ammonia decomposition is shown in Table 2. Ammonia conversion increases with the initial increment of the DP time, and then a maximum appears at 3 h. Further increasing of the DP time reduces ammonia conversion. As validated by the XRF

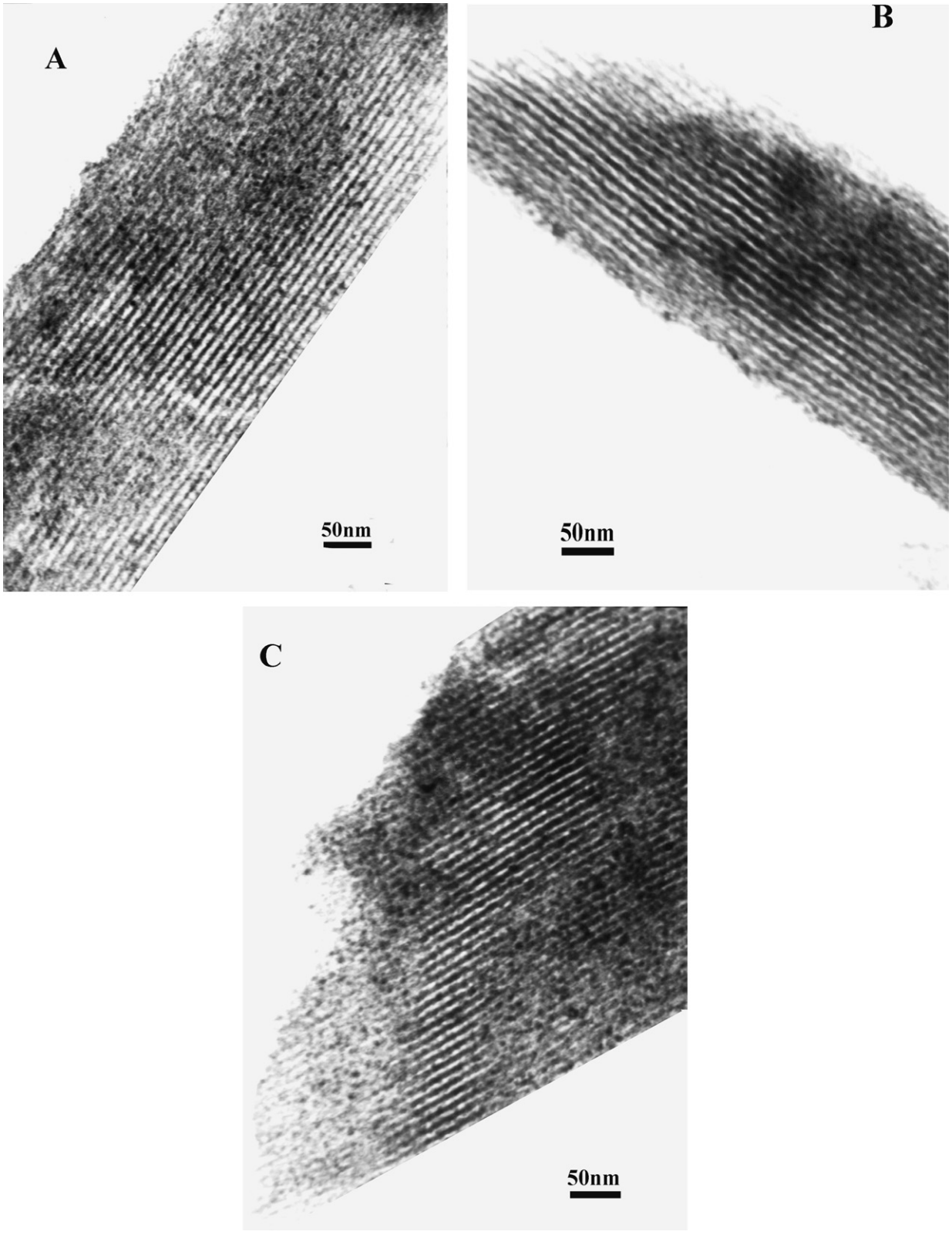

Fig. 8. TEM images of catalysts reduced under different temperatures. (A) 573 K, (B) 873 K and (C) 923 K.

experiment (Table 1), the amount of nickel deposited on SBA-15 increases with the DP time, whereas the nickel surface area of Ni/SBA-15(4) is lower than that of Ni/SBA-15(3) based on the results of H_2-pulse chemisorption, indicating that the formation of more buried nickel sub-layers that are inaccessible by the reactants. This might be the main reason that caused the decrease of ammonia conversion when the DP time is more than 3 h.

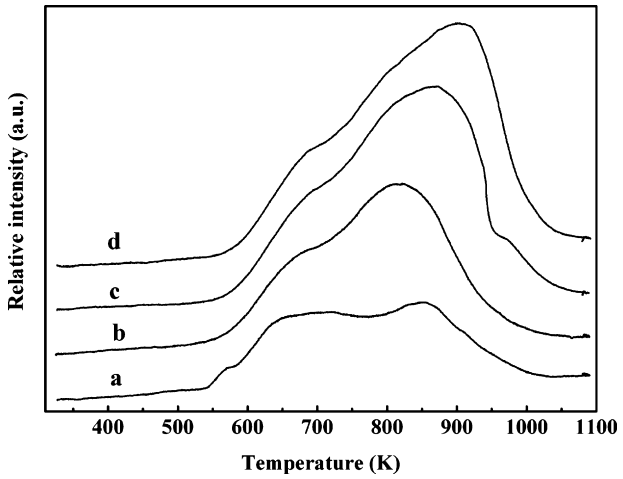

Fig. 9. H_2-TPR curves of Ni-based samples calcinated at 823 K for 3 h. (a) 10% Ni/SBA-15(r), (b) Ni/SBA-15(2), (c) Ni/SBA-15(3) and (d) Ni/SBA-15(4).

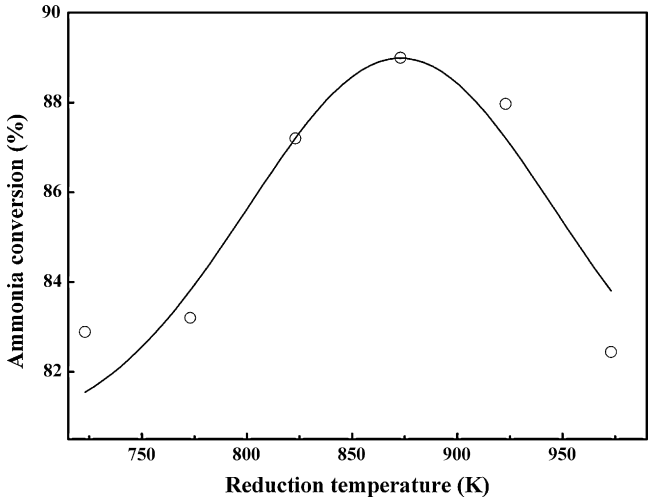

Fig. 10. Catalytic performance of Ni/SBA-15(3) reduced at different temperatures (reaction temperature = 823 K, $GHSV_{NH_3}$ = 30,000 ml/h g-cat).

3.2.2. Effect of reduction temperature on catalytic performance

Fig. 10 shows the influence of reduction temperature on catalytic performance when reaction temperatures are 823 K with $GHSV_{NH_3}$ of 30,000 ml/h g-cat. Ammonia conversion increased first with the reduction temperature; a maximum around 89% could be obtained at 873 K and then the conversion decreased. It could be noted from Fig. 9 that, as for Ni/SBA-15(3), the reduction temperatures need to be above 973 K when nickel phases deposited on SBA-15 are fully reduced. Our investigations found that the reduction is incomplete at lower temperatures. The increase of catalytic performance at lower reduction temperatures might be due to the rise of reduction extent with rising of reduction temperature. On the other hand, ammonia conversion did not increase with increasing of reduction temperatures when the temperature is above 873 K, but rather decreased, indicating that the effect of the reduction extent is not the unique factor in determining the activity of catalyst. It is known from XRD patterns and TEM images that the morphology of nickel particles changes with increasing reduction temperature. A certain particle size of nickel will promote the activity of Ni/SBA-15, since ammonia decomposition is a structure-sensitive reaction. Previous investigations [11,31–33] also provided abundant information elucidating the relationship between the activity of ammonia decomposition and the morphology of active components.

3.2.3. Effect of reaction temperature and $GHSV_{NH_3}$ on catalytic performance

Fig. 11 depicts the effect of reaction temperature and $GHSV_{NH_3}$ on performance of Ni/SBA-15(3). One can see that the ammonia conversion increases with the reaction temperature, in agreement with the mild endothermic reaction of ammonia catalytic decomposition. From Fig. 11, it can be seen when the $GHSV_{NH_3}$ is raised from 11,000 to 46,000 ml/h g-cat, ammonia conversion decreases from 93% to 83%, indicating that relatively low $GHSV_{NH_3}$ is beneficial to ammonia decomposition on Ni/SBA-15 catalysts. Even so, at $GHSV_{NH_3}$ of 46,000 ml/h g-cat and 873 K, above 96% ammonia conversion could be obtained.

3.2.4. Catalytic performance comparison of samples prepared with different methods

The performance of catalysts prepared by the DP method and by the impregnation method were investigated under identical reaction conditions. Table 3 shows catalytic performance comparison of samples prepared by different methods at 823 K with $GHSV_{NH_3}$ of 30,000 ml/h g-cat. The table shows that ammonia conversion and hydrogen formation rate over the Ni/SBA-15 prepared by the DP method is much higher than that over the Ni/SBA-15 catalysts obtained using the impregnation method. From Table 4, one can see that the ammonia conversion and hydrogen formation rate over Ni/SBA-15(3)

Table 2
Ammonia conversion (%) and H_2 formation rate (mmol/min g_{cat}) over the Ni/SBA-15 catalysts prepared by deposition–precipitation method[a]

Temperature (K)	Ni/SBA-15(2)		Ni/SBA-15(3)		Ni/SBA-15(4)	
	Conversion	Rate (H_2)	Conversion	Rate (H_2)	Conversion	Rate (H_2)
723	24.2	8.1	28.3	9.5	25.0	8.4
773	49.1	16.4	57.0	19.1	52.1	17.4
823	74.5	24.9	82.2	27.5	80.1	26.8
873	92.1	30.8	96.2	32.2	95.2	31.9
893	95.9	32.1	98.6	33.0	97.6	32.7
923	98.7	33.1	99.7	33.4	99.2	33.2

[a] All catalysts were reduced at 773 K for 5 h.

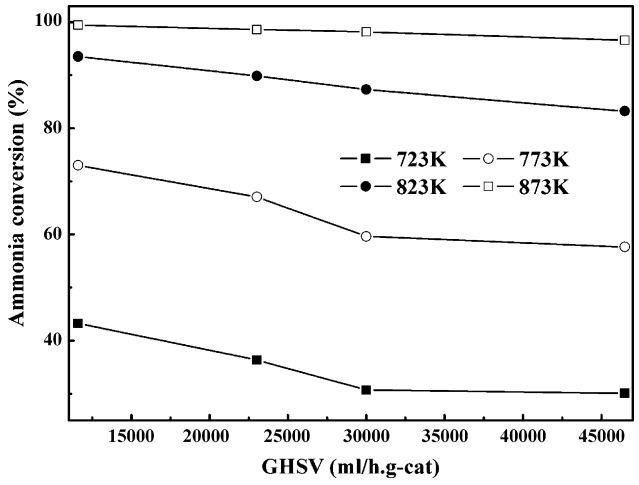

Fig. 11. Effect of reaction temperature and $GHSV_{NH_3}$ on catalytic performance of Ni/SBA-15(3) (the catalyst was reduced at 873 K for 5 h).

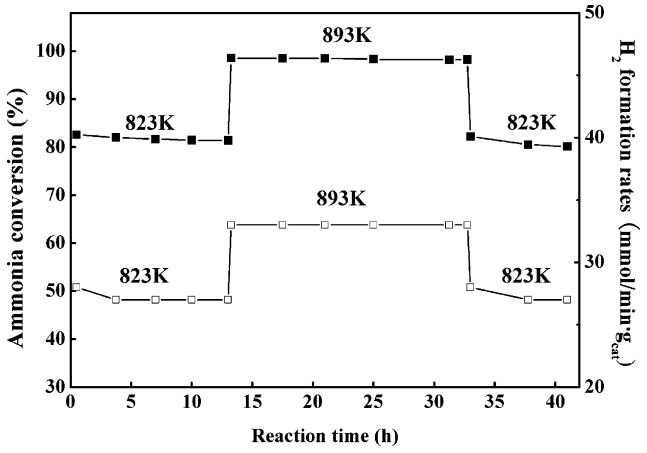

Fig. 12. Stability of Ni/SBA-15(3) catalyst.

Table 3
Ammonia conversion (%) and H_2 formation rate (mmol/min g-cat) over catalysts prepared with different methods at 823 K with $GHSV_{NH_3}$ of 30,000 ml/h g-cat

Catalyst	Preparation method	Conversion	Rate (H_2)	Reference
10% Ni/SBA-15(r)	Impregnation	50.8	17.0	This study
Ni/SBA-15(3)	Deposition–precipitation	89.0	29.8	This study
Ni/SiO_2	Impregnation	21.6	6.8	[2]
$Ni/SiO_2/Al_2O_3$	Impregnation	48.7	15.2	[2]
Ni/Al_2O_3	Coprecipitation	75.0	25.1	[10]
Ni/SiO_2	Impregnation	34.6	11.6	[12]
Ni/MCM-41	Impregnation	44.6	14.9	[12]
Ni/MCM-41	Template ion-exchange	47.6	15.9	[12]
Ni/SBA-15	Impregnation	37.8	12.7	[12]
Ru/AC	Impregnation	78.9	26.4	[7]
Ru/ZrO_2	Impregnation	77.0	25.8	[7]
Ru/Al_2O_3	Impregnation	73.7	23.5	[7]
Ru/SBA-15	Impregnation	93.3	31.2	[12]

catalyst are higher than other Ni-based catalysts prepared using the coprecipitation method [10,11] and template ion-exchange method [12], and even superior to some supported Ru catalysts. The values are only slightly lower than those for the Ru/SBA-15.

Undoubtedly, the preparation method is one of major factors that should be responsible for the catalytic performance. As for the Ni/SBA-15(3) sample, the small nickel particle sizes around 5 nm and high dispersion above 20% could be achieved, whereas the nickel particle size of 10% Ni/SBA-15(r) catalyst is larger than 100 nm and the dispersion is only around 0.9%. This might be the main reason that causes the high activity of Ni/SBA-15 catalysts prepared by the DP method.

3.3. Catalytic stability

Fig. 12 shows the investigation of stability of the Ni/SBA-15(3) catalysts. Ammonia conversion and H_2 formation rates over the Ni/SBA-15(3) catalyst remained unchanged even at 893 K for 24 h. Such results demonstrate that the catalysts prepared by the DP method are stable, which could be attributed to the strong interaction of active components with the supports to prevent small particles of active components from sintering [19]. Additionally, it is worth pointing out that the catalyst has been reduced in a flow of 1:3 H_2–He at 773 K for 5 h prior to the measurement of catalytic activity.

4. Conclusion

Ni/SBA-15 catalysts prepared by using DP methods show high activity and stability for ammonia decomposition to produce CO_x-free hydrogen. The pore structure of SBA-15 has been retained through the DP preparation process followed with calcination and reduction, though the DP time has a significant effect on the textural properties. The small nickel particle size, higher dispersion and high resisting sintering would be responsible for the higher catalytic performance and stability of Ni/SBA-15 catalysts prepared with DP method.

Ammonia conversion over the Ni/SBA-15 catalysts is above 96% at 873 K with $GHSV_{NH_3}$ of 46,000 ml/h g-cat, which is much higher than the values for other Ni-based catalysts, even higher than the values for some Ru-based catalysts. This

material is a prospective candidate for practical application in the field of producing CO_x-free hydrogen from ammonia decomposition.

References

[1] A.S. Chellappa, C.M. Fisher, W.J. Thomson, Appl. Catal. A 227 (2002) 231–240.
[2] T.V. Choudhary, C. Sivadinarayana, D.W. Goodman, Catal. Lett. 72 (3/4) (2001) 197–201.
[3] J.N. Armor, Appl. Catal. A 176 (1999) 159–176.
[4] R. Metkemeijer, P. Achard, Int. J. Hydrogen Energy 19 (1994) 535–542.
[5] R. Metkemeijer, P. Achard, J. Power Sources 49 (1994) 271–282.
[6] D. Szmigiel, W. Raróg-Pilecka, E. Miśkiewicz, Z. Kaszkur, Z. Kowalczyk, Appl. Catal. A 264 (2004) 59–63.
[7] S.F. Yin, Q.H. Zhang, B.Q. Xu, W.X. Zhu, C.F. Ng, C.T. Au, J. Catal. 224 (2004) 384–396.
[8] S.F. Yin, B.Q. Xu, S.J. Wang, C.F. Ng, C.T. Au, Catal. Lett. 96 (3/4) (2004) 113–116.
[9] S.F. Yin, B.Q. Xu, C.F. Ng, C.T. Au, Appl. Catal. B 48 (2004) 237–241.
[10] J. Zhang, H.Y. Xu, X.L. Jin, Q.J. Ge, W.Z. Li, Appl. Catal. A 290 (2005) 87–96.
[11] J. Zhang, H.Y. Xu, W.Z. Li, Appl. Catal. A 296 (2005) 257–267.
[12] X.K. Li, W.J. Ji, J. Zhao, S.J. Wang, C.T. Au, J. Catal. 236 (2005) 181–189.
[13] H.C. Liu, H. Wang, Z.M. Liu, J.H. Shen, in: Proceedings of the 13th International Congress on Catalysis, Paris, France, (2004), pp. 4–102.
[14] H.C. Liu, H. Wang, J.H. Shen, Y. Sun, Z.M. Liu, Petrochem. Technol. 34 (Suppl.) (2005) 495–497.
[15] C.H. Liang, W.Z. Li, Z.B. Wei, Q. Xin, C. Li, Ind. Eng. Chem. Res. 39 (2000) 3694–3697.
[16] J.W. Geus, J.A.R. van Veen, Stud. Surf. Sci. Catal. 123 (1999) 459–485.
[17] P. Burattin, M. Che, C. Louis, J. Phys. Chem. B 101 (1997) 7060–7074.
[18] P. Burattin, M. Che, C. Louis, J. Phys. Chem. B 102 (1998) 2722–2732.
[19] P. Burattin, M. Che, C. Louis, J. Phys. Chem. B 103 (1999) 6171–6178.
[20] P. Burattin, M. Che, C. Louis, J. Phys. Chem. B 104 (2000) 10482–10489.
[21] D.Y. Zhao, J.L. Feng, Q.S. Huo, N. Melosh, G.H. Fredrickson, B.F. Chmelka, G.D. Stucky, Science 279 (1998) 548–552.
[22] R. Gómez-Reynoso, J. Ramírez, R. Nares, R. Luna, F. Murrieta, Catal. Today 107/108 (2005) 926–932.
[23] Y.M. Liu, Y. Cao, S.R. Yan, W.L. Dai, K.N. Fan, Catal. Lett. 88 (2003) 61–67.
[24] B. Solsona, T. Blasco, J.M.L. Nieto, M.L. Peña, F. Rey, A. Vidal-Moya, J. Catal. 203 (2001) 443–452.
[25] L. Vradman, M.V. Landau, M. Herskowitz, V. Ezersky, M. Talianker, S. Nikitenko, Y. Koltypin, A. Gedanken, J. Catal. 213 (2003) 163–175.
[26] R. Nares, J. Ramírez, A. Gutiérrez-Alejandre, C. Louis, T. Klimova, J. Phys. Chem. B 106 (2002) 13287–13293.
[27] C.P. Li, Y.W. Chen, Therm. Acta 256 (1995) 457–465.
[28] A. Roman, B. Delmon, J. Catal. 30 (1973) 333–342.
[29] B. Mile, D. Stirling, M.A. Zammitt, A. Lovell, M. Webb, J. Catal. 114 (1988) 217–229.
[30] A. Díaz, D.R. Acosta, J.A. Odriozola, M. Montes, J. Phys. Chem. B 101 (1997) 1782–1790.
[31] A. Jedynak, Z. Kowalczyk, D. Szmigiel, W. Rarog, J. Zieliński, Appl. Catal. A 237 (2002) 223–226.
[32] W. Raróg-Pilecka, D. Szmigiel, A. Komornicki, J. Zieliński, Z. Kowalczyk, Carbon 41 (2003) 589–591.
[33] S. Dahl, E. Törnqvist, I. Chorkendorff, J. Catal. 192 (2000) 381–390.